Journal of Controlled Release 357 (2023) 210–221

Contents lists available at ScienceDirect

Journal of Controlled Release

journal homepage: www.elsevier.com/locate/jconrel

Metal coordination micelles for anti-cancer treatment by gene-editing and phototherapy

Chen Zhang [a], Xiaojie Wang [a], Gengqi Liu [a], He Ren [a], Jiexin Li [a], Zhen Jiang [a], Jingang Liu [a], Jonathan F. Lovell [b], Yumiao Zhang [a,*]

[a] Key Laboratory of Systems Bioengineering (Ministry of Education), Frontiers Science Center for Synthetic Biology (Ministry of Education), School of Chemical Engineering and Technology, Tianjin University, Tianjin 300350, P. R. China
[b] Department of Biomedical Engineering, The State University of New York at Buffalo, Buffalo, NY 14260, United States

ARTICLE INFO

Keywords:
CRISPR/Cas9
Manganese coordination
Dual guide RNA
Responsive release
Antitumor

ABSTRACT

CRISPR-Cas9 is a central focus of the emerging field of gene editing and photodynamic therapy (PDT) is a clinical-stage ablation modality combining photosensitizers with light irradiation. But metal coordination biomaterials for the applications of both have rarely been investigated. Herein, Chlorin-e6 (Ce6) Manganese (Mn) coordination micelles loaded with Cas9, termed Ce6-Mn-Cas9, were developed for augmented combination anticancer treatment. Manganese played multiple roles to facilitate Cas9 and single guide RNA (sgRNA) ribonucleoprotein (RNP) delivery, Fenton-like effect, and enhanced endonuclease activity of RNP. Histidine (His)-tagged RNP could be coordinated to Ce6 encapsulated in Pluronic F127 (F127) micelles by simple admixture. Triggered by ATP and endolysosomal acidic pH, Ce6-Mn-Cas9 released Cas9 without altering protein structure or function. Dual guide RNAs were designed to target the antioxidant regulator MTH1 and the DNA repair protein APE1, resulting in increased oxygen and enhanced PDT effect. In a murine tumor model, Ce6-Mn-Cas9 inhibited tumor growth with the combination therapy of PDT and gene editing. Taken together, Ce6-Mn-Cas9 represents a new biomaterial with a high degree of versatility to enable photo- and gene-therapy approaches.

1. Introduction

Metal ions play an important role in tumor therapy including in DNA damage [1,2], and metalloimmunotherapy [3,4]. Metal ions have been widely used as cofactors to promote gene editing efficacy of various nucleic acid tools such as DNAzyme [5,6], siRNA [7,8], miRNA [9] and other materials for nucleic acid cleavage [10]. As an emerging gene editing technology, the cluster regularly interspaced short palindromic repeat (CRISPR)-associated protein (Cas9) system has gained a great deal of attention, but there have been relatively few metal ion-oriented biomaterials for CRISPR/Cas9 delivery. Simulations have shown that Mg^{2+}, Mn^{2+} and Ca^{2+} can activate the HNH conformation and change the catalytic state of Cas9 [11]. For example, it was reported that manganese ions (Mn^{2+}) as a cofactor could improve the gene editing effect of Cas9 [12], however, therapeutic applications of Mn^{2+}-related Cas9 gene editing material have rarely been investigated to our knowledge. Mn^{2+} is particularly interesting since as a transition metal ion, it can catalyze H_2O_2 with low oxidation capacity through Fenton or Fenton-like reactions [13,14], which are used in chemodynamic therapy [15–17]. One of the challenges for CRISPR-Cas9 delivery technology is that the connection between Cas9 and carriers might alter protein conformation, leading to impaired gene-editing performance. Metal ions could be anchored to His-tagged Cas9 via the coordination interaction [18,19]. This approach has the advantages of simple preparation, strong stability and high encapsulation efficiency [20,21]. More importantly, metal chelation does not impair catalytic activity of Cas9 [22]. The combination of Mn^{2+} can not only increase the gene editing performance of Cas9, but also provide a safe and effective solution for the basis of CRISPR/Cas9 scaffolding structures. As such, augmented anti-tumor efficacy by combining gene edit and chemodynamic therapeutic strategies could be realized.

Photodynamic therapy (PDT) has been used as a promising approach to treat tumors, involving use of light to trigger photosensitizers and generate reactive oxygen species (ROS) for killing tumor cells [23–25]. In this study we show that, His-tagged Cas9 can bind to the Ce6 photosensitizer through the coordination interaction between His-tags

* Corresponding author.
E-mail address: ymzhang88@tju.edu.cn (Y. Zhang).

https://doi.org/10.1016/j.jconrel.2023.03.042
Received 16 September 2022; Received in revised form 8 March 2023; Accepted 23 March 2023
Available online 5 April 2023

and Mn^{2+} chelated in Ce6, realizing a combination treatment strategy of gene therapy and photodynamic therapy [26–28]. It has been reported that MutT homolog 1 (MTH1) protein can remove oxidized nucleotides and prevent high levels of ROS from causing damage to proliferating tumor cells [29,30]. However, tumor cells are usually in a hypoxic microenvironment owing to rapid tumor growth supported by tortuous blood vessels [31,32], which also hampers the production of ROS leading to suboptimal PDT outcomes. Human apurinic endonuclease 1 (APE1) is associated with mitochondrial function and low expression of APE1 results in increased intracellular oxygen accumulation [33,34]. To this end, CRISPR/Cas9 could be mediated by sgRNAs to decrease the expression of MTH1 and APE1, resulting in increased intracellular oxygen by interfering cellular oxidative defense system. Since transition metals could chelate with chlorin e6 (Ce6) or His-tagged Cas9 via coordination, and Cas9 coordination and release could be achieved in response to pH and adenosine triphosphate (ATP) stimuli in tumors in a spatiotemporal manner [35,36]. Metal coordination nanoparticles comprising photosensitizer, metal and Cas9 could found widespread use in combined gene and photodynamic therapy for synergistic anti-tumor treatment. Such combination therapy ablates cancer cells more efficiently [37,38], and also shortens the treatment duration since gene therapy alone typically needs longer treatment times for efficacy [39,40].

Herein, we developed a CRISPR/Cas9 delivery system using Ce6 encapsulated Pluronic (Poloxamer) F127 micelles, termed Ce6-Mn-Cas9 for synergistic cancer treatment. As depicted in Scheme 1, Mn^{2+} as a bridge enables His-tagged Cas9 to anchor onto Ce6 micelles via the coordination without changing conformation and gene-editing properties of Cas9. After internalization by tumor cells, Ce6-Mn-Cas9 have ability to escape from lysosomes in response pH and ATP in tumor cells. In addition to the generation of Fenton-like effect, Mn^{2+} was also found to act as a cofactor of Cas9 to promote gene editing activity. We designed dual guide RNAs to target MTH1 and APE1 to simultaneously inhibit the tumor cell repair and enhance oxygen accumulation, resulting in reprogrammed tumor microenvironment and enhanced anti-tumor efficacy by the combination of photo and gene therapy.

2. Experimental materials and methods

2.1. Materials

Chlorin-e6 was purchased from Sigma (USA). *P*-nitrophenyl chloroformate, 1-(3-dimethylaminopropyl)-3-ethylcarbodiimide hydrochloride, 4-dimethyla minopyridine, Tris (2-carboxyethyl) phosphine hydrochloride and methy-β-cyclodextrim were obtained from Heowns (China). SgRNA was produced by Genewiz (Suzhou, China). Roswell Park Memorial Institute 1640 (RPMI-1640) and Dulbecco's Modified Eagle Medium (DMEM) growth medium, fetal bovine serum (FBS) and penicillin/streptomycin were purchased from Gibco (USA). Dialysis tubing (molecular weight cut off: 300,000 Da) was obtained from Viskase (USA). 4,6-diamidino-2-phenylindole dihydrochloride (DAPI) were purchased from Invitrogen (USA). Bicinchoninic acid (BCA) protein assay kit, protein marker, DNA ladder and fluorescein isothiocyanate (FITC) were obtained from Solarbio Science & Technology (Beijing, China). All the antibodies were purchased from Sangon Biotech (Shanghai, China). All ultra-centrifugal filtration devices were obtained from Millipore (USA). Cell Counting Kit-8 (CCK-8), Lysosome tracker, YF488-Annexin V/PI kit and cytotoxicity assay kit for animal cells were purchased from US everbright (China).

2.2. Expression and endonuclease activity of Cas9

Cas9 protein was expressed by *E. coli* containing pET-28b-Cas9 plasmid, followed by typical protein purification procedure [41]. After

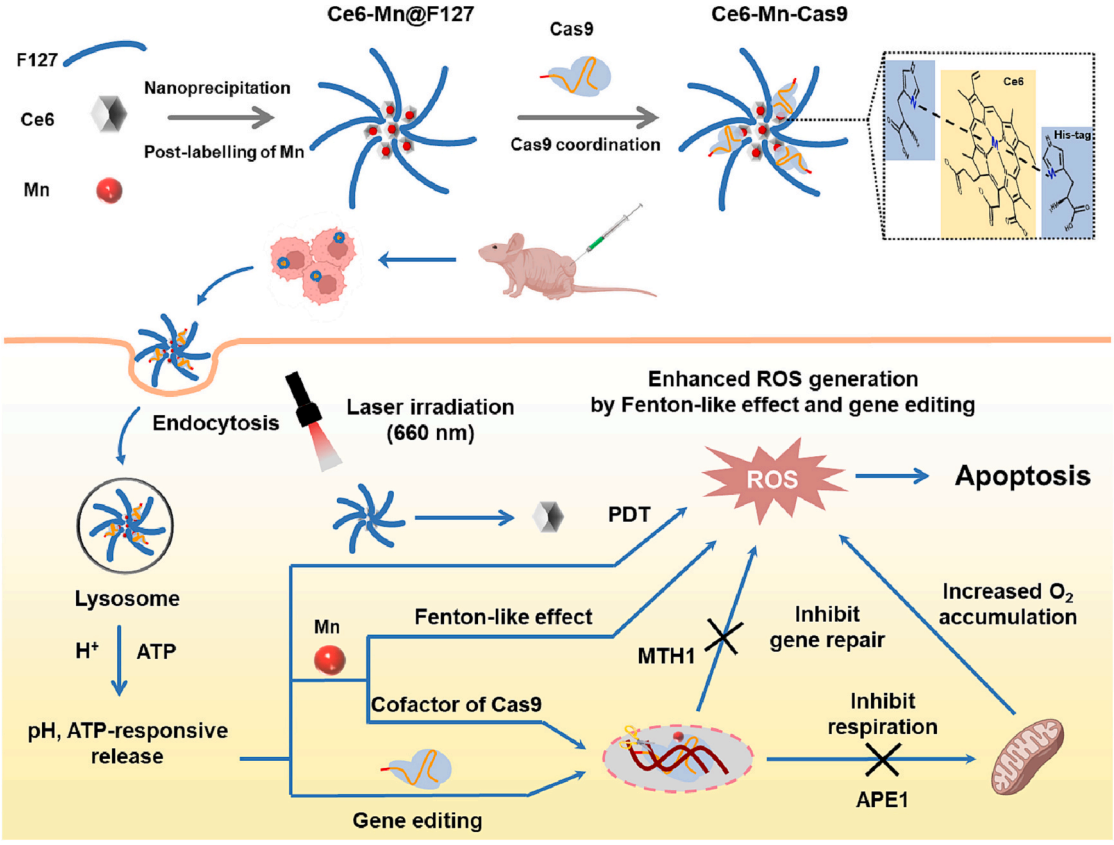

Scheme 1. Illustration of the preparation of Ce6-Mn-Cas9-MTH1 + APE1 and its mechanism for enhanced anti-tumor efficacy, in combination with gene editing and photodynamic therapy.

purification with 30 kDa ultrafiltration tube for three times, the samples were quantified by BCA Protein Assay Kit and stored in buffer (50 mM Tris, 200 mM KCl, 0.1 mM EDTA, 10% glycerol) at −80 °C. To verify the endonuclease activity of Cas9, the purified Cas9 protein was incubated with EGFP sgRNA at a molar ratio of 1:1 for 10 min. The resulting RNP was added to a 7 μL reaction solution containing water, EGFP dsDNA, and a metal ion buffer. The reaction system was placed at 37 °C for 30 min and analyzed by 2% agarose gel electrophoresis. EGFP sgRNA sequence: 5′-ccggcaagctgcccgtgccc-3′. Scaffold sequence: 5′-gttttagagctagaaatagcaagttaaaataaggctagtccgttatcaacttgaaaaagtggcaccgagtcggtgc-3′. The catalytic activity of Cas9 in the presence of metal ions with different concentrations followed the same procedure above.

In order to evaluate the integrity and remaining endonuclease activity of Cas9 protein after laser treatment, Ce6-Mn-Cas9 micelles were prepared with Cas9 concentration of 0.1 mg mL^{-1} and a molar ratio of Ce6 to Cas9 of 10:1. After treatment by laser (660 nm, 0.1 W cm^{-2}, 1 min), they were subjected to circular dichroism analysis. Circular dichroism spectra (CD) were performed by a J-810 spectro-polarimeter (Jasko, Germany) using a 0.2 mm thick quartz cuvette for measurements. In addition, the solution with or without laser treatment was placed at 37 °C for 30 min after laser irradiation and then the endonuclease activity was analyzed by 2% agarose gel electrophoresis.

2.3. Synthesis of metal-chelated Ce6 in F127 micelles

Chlorin e6 (1 mg, 1. 68 mmol,1 eq) was dissolved in 1 mL tetrahydrofuran and added into 10 mL 10% (wt) Pluronic F127, F68 or F108 aqueous solution, followed by sonication for 30 min. After it was fully dissolved, it was placed on a magnetic stirrer and then added different metal chloride (100 eq) which was dissolved in 60 μL sodium acetate aqueous solution and stirred sequentially overnight. The obtained liquid was eluted by ultrafiltration (MWCO: 100 kDa) for three times and then collected for further analysis. Ce6 absorbance was quantified by spectrophotometer, according to the measured standard curve. To quantify Ce6, micellar Ce6 was dissolved in tetrahydrofuran (THF) with volume ratio of 1:9, followed by absorbance measurement. Standard curve in Fig. S1 was made by dissolving Ce6 with indicated concentrations in solution of THF(water: tetrahydrofuran(v v^{-1}) = 1:9). To quantify concentration of metal ions, 1 mL metal-chelated Ce6 in F127 micelles solution was taken for aqua regia digestion (a mixture of concentrated hydrochloric acid (HCl) and concentrated nitric acid (HNO_3) at a volume ratio of 3:1). Then the solutions were diluted to 5 mL with water for the following ICP-OES (iCAP7000 series) analysis for quantification.

2.4. Synthesis of Ce6-metal-Cas9

To chelate Cas9 onto micelles, Ce6-Metal@F127 (quantified by the amount of Ce6) were simply admixed with Cas9 aqueous solution in a molar ratio of 10 (Ce6) to 1 (Cas9). After chelation at 4 °C for 12 h, the yield was calculated by measuring the fluorescence intensity of FITC labeled Cas9. To verify successful chelation, Ce6-Metal-Cas9 were treated by 250 mM imidazole and 10% (v v^{-1}) Triton X-100 solution for 10 h, followed by ultracentrifugation to remove de-chelated Cas9. The obtained fluorescence in retentate was quantitatively analyzed with a microplate reader.

2.5. Ce6-metal-Cas9 characterization

The morphology of Ce6-Mn-Cas9 and Ce6-Ni-Cas9 were characterized using transmission electron microscopic (JEM-F200 or JEM-1400, JEOL, Japan) and Energy Dispersive Spectroscopy (EDS) analysis was also performed on the same instrument. The hydrodynamic dimensions of Ce6-metal@F127 and Ce6-metal-Cas9 were measured by Zetasizer nano zs90 (Malvern instruments, Malvern, UK). To test the stability of Ce6-Metal-Cas9, the prepared micelles were added in a dialysis bag (MWCO: 300 kDa) and dialyzed against a 10% (v v^{-1}) fetal bovine serum (FBS) solution. 20 μL solution in dialysis bag was taken every 2 h for fluorescence quantification to quantify the remaining FITC labeled Cas9 in dialysis bag.

2.6. FRET

The synthesis of F127-NH_2 was synthesized according to previously published protocol [42]. Cas9 was stained with Cy3 and F127-NH_2 was conjugated by Cy5 via ester bonds, followed by removal of free fluorescence dyes by dialysis. Ce6-Mn@F127 was added to Cas9 at a molar ratio of 10 (Ce6) to 1 (Cas9) and incubated for 12 h. Then the fluorescence of formulations as indicated was measured by a microplate reader in Fig. 1e.

2.7. $^1O_2$ generation in vitro

For evaluating the $^1O_2$ generation of Ce6-Mn-Cas9 and Ce6-Ni-Cas9 under laser irradiation, 1, 3-diphenylisobenzofuran (DPBF) was employed as the $^1O_2$ indicator in Fig. 2d. DPBF in DMSO solution (10 μM) was added to Ce6-Ni@F127 (50 μg mL^{-1}) and Ce6-Mn@F127 solutions (50 μg mL^{-1}). After irradiating the mixture with laser (660 nm, 0.1 W cm^{-2}) for (0, 2, 4, 6, 8, 10, 12 min) as indicated, the characteristic UV–Vis absorption spectra of DPBF were measured. Moreover, the capturing agent 2,2,6,6-tetramethylpiperidine (TEMP), was used to detect the generation of $^1O_2$ via the ESR spectrometer (Brooker A300) in Fig. 2e.

2.8. OH generation detection in vitro

For the methylene blue (MB) degradation experiment, Ce6-Ni@F127 and Ce6-Mn@F127 with concentrations of 50 μg mL^{-1} were incubated respectively with 25 mM $NaHCO_3$ aqueous solution, 10 μg mL^{-1} MB and 1 mM H_2O_2 at 37 °C for 4 h. Then the absorbance was measured at a wavelength from 400 to 800 nm by spectrophotometer in Fig. 2f.

2.9. pH and ATP-triggered release of Cas9 in vitro

The prepared Ce6-Mn-Cas9 and Ce6-Ni-Cas9 were poured to a 300 kDa dialysis bag and soaked in 0.1 mM or 10 mM ATP solution, and placed in an incubator at 37 °C, followed by sampling the liquid in the dialysis bag at a specified time as indicated for protein quantification by BCA Protein Assay Kit. The size of samples before and after treatment by ATP solutions was measured. And agar gel electrophoresis and sodium lauryl sulfate polyacrylamide gel electrophoresis were also conducted. The pH release profile at pH 5.5 or 7.4 was also studied by the same protocol above. Data were exhibited in Fig. 2g-i and S5.

To investigate whether Mn^{2+} was released in the acidic condition, Ce6-Mn-Cas9 micelles were prepared with Mn^{2+} concentration of 0.01 mg mL^{-1} and Cas9 concentration of 0.012 mg mL^{-1}. They were dialyzed (MWCO: 8000–12,000 Da) against pH = 5.5 or PBS solution for 12 h, the retentate was collected for the measurement of Mn by ICP-OES (iCAP7000 series) analysis.

2.10. Cellular cytotoxicity and uptake of micelles

NIH-3 T3 and HEK-293 cells were placed in a 96-well cell culture plate with 2×10^5 cells per well and cultured overnight. Ce6-Mn-Cas9 or Ce6-Ni-Cas9 were added and incubated for 12 h. Herein, the amount of Cas9 is 1.75 μg per well and the molar ratio of Ce6 to Cas9 was 10 to 1. After washing with phosphate buffered solution (PBS) for three times, cell viability was assessed by cell counting kit-8 (CCK-8) assay. A549 cells were divided into four groups: 1 PBS, 2 free Cas9, 3 Ce6-Mn-Cas9 and 4 Ce6-Ni-Cas9 for cellular uptake by measuring the fluorescence of FITC-labeled Cas9. The cell nuclei and lysosomes were stained by 4′,6-diamidino-2-phenylindole (DAPI) and Lyso Tracker Red, respectively,

and the intracellular distribution of Ce6-Mn-Cas9 and Ce6-Ni-Cas9 was imaged by CLSM in Fig. 3a and b.

2.11. Cellular uptake pathway determination

Ce6-Mn-Cas9 with Cas9 labeled by FITC was added into 96-well (1.75 μg Cas9 per well and the molar ratio of Ce6 to Cas9 was 10 to 1) or 6-well plates (28 μg Cas9 per well and the molar ratio of Ce6 to Cas9 was 10 to 1) containing 1×10^5 or 1×10^6 A549 cells in each well, followed by incubation for 4 h. The cells were treated with Methyl-β-cyclodextrin (MβCD, 7.5 mg mL^{-1}), 5-(*N*, *N*-Hexamethylene)amiloride (0.6 mg mL^{-1}) or low temperature (4 °C) overnight, and the fluorescence intensity was determined by flow cytometry in Fig. 3c.

2.12. EGFP gene targeting assay

To evaluate the genome-editing ability of Ce6-Ni-Cas9-EGFP and Ce6-Mn-Cas9-EGFP, 5×10^5 A549 cells expressing EGFP in 6-well plate were used in this study and treated by (I) PBS, (II) free Cas9-EGFP (28 μg Cas9, molar ratio of Cas9 to sgRNA was 1:2), (III) Ce6-Ni-Cas9-EGFP (28 μg Cas9), and (IV) Ce6-Mn-Cas9-EGFP (28 μg Cas9) groups. After 72 h, they were washed twice with cold PBS and then the remaining EGFP after gene cutting by various formulations was assessed by CLSM observation and flow cytometry analysis in Fig. 3d and f.

2.13. Detection of intracellular ROS

The A549 cells were treated by (I) PBS, (II) free Cas9 (III) Ce6-Mn-Cas9 + laser irradiation, (IV) Ce6-Ni-Cas9 + laser irradiation. A549 cells were incubated with various samples at 37 °C for 12 h. Here, the amount of Cas9 is 28 μg per well in 6-well plate and the molar ratio of Ce6 to Cas9 was 10 to 1. After washing by PBS for three times, groups (II), (IV) and (VI) were treated by 2′, 7′- dichlorodihydrofluorescein diacetate (DCFH-DA) (10 μM), and laser irradiation (660 nm, 0.1 W cm^{-2}, 5 min). After further incubation for 3 min, the intracellular ROS generation in these groups was assessed by CLSM observation and then the fluorescence of formulations as indicated was measured by a microplate reader in Fig. 3g. Excitation wavelength: 480 nm, emission wavelength: 400–650 nm.

2.14. PDT effect in vitro

To optimize the experimental conditions for PDT, the A549 cells were incubated with Ce6 aqueous solution with a final concentration of 3 μg (Ce6) mL^{-1} for 6 h, followed by irradiation by 660 nm laser for different durations (0, 1, 2, 3, 4, 5, 8, 10 and 15 min). After culturing overnight, Ce6 aqueous solution was washed with PBS, and CCK-8 solution was added. UV spectrophotometer was used to measure the absorbance at 450 nm. After the appropriate irradiation time was determined, Ce6 aqueous solution with different concentrations of 0, 0.05, 0.1, 0.5, 1, 2, 5 μg (Ce6) mL^{-1} was added to A549 cells. The concentration of Ce6-Mn-Cas9-MTH1 + APE1 was 0.5 μg (Ce6) mL^{-1}. After incubation for 6 h, laser irradiation (660 nm, 0.1 W cm^{-2}, 5 min) was shed on cells and the detection method was the same as above in Fig. 4b. Molar ratio of Ce6 to Cas9 was 10:1.

2.15. Cell killing experiment

To detect cancer cell apoptosis induced by various formulations in Fig. 4c, A549 cells were seeded in 96-well plates and cultured overnight. A549 cells were treated by the following formulations (a) PBS, (b) Ce6-Mn-Cas9-MTH1, (c) Ce6-Mn-Cas9-APE1 and (d) Ce6-Mn-Cas9 -APE1 + MTH1 (the amount of Cas9 is 1.75 μg per well) for 72 h. Each group was treated by dark or laser irradiation (660 nm, 0.1 W cm^{-2}, 5 min) as indicated. After the cells were incubated for 72 h, CCK-8 solution was added and the cells were incubated for another 1 h, then the absorbance at 450 nm was measured.

For the cell apoptosis experiment, the cells were placed in a 6-well plate with a density of 5×10^4 and the amount of Cas9 is 28 μg per well, followed by incubation overnight. Cells were then treated with PBS, free Cas9-MTH1 + APE1, Ce6-Ni-Cas9-MTH1 + APE1 and Ce6-Mn-Cas9-MTH1 + APE1. After 6 h, the cells were irradiated with laser (660 nm, 0.1 W cm^{-2}, 5 min). After culture overnight, the cells were collected and stained with calcein-AM/PI (10 μL) solution for 30 min, followed by CLSM observation in Fig. 4d. Cell viability staining was the same as the above procedure, and the cells were stained by PI and then analyzed by flow cytometry in Fig. 4e.

2.16. Western blotting analysis

First, A549 cells were treated with Ce6-Mn-Cas9 or Ce6-Mn-Cas9 for 12 h. Herein, the amount of Cas9 is 28 μg per well in 6-well plate and the molar ratio of Ce6 to Cas9 was 10 to 1. Subsequently, the cells were irradiated with laser (660 nm, 0.1 W cm^{-2}) for 10 min. After 12 h, the cells were rinsed by PBS and treated with radio immunoprecipitation assay (RIPA) lysis buffer with 1 mM phenylmethanesulfonyl fluoride (PMSF) for 30 min. Subsequently the lysis solution was centrifuged and the supernatant was collected for quantitative analysis by a BCA protein assay Kit. The 20 μL of protein samples were separated by SDS-PAGE gel electrophoresis and then transferred to a nitrocellulose membrane. After rinsing with Tris Buffered Saline with Tween (TBST), the membrane was sealed with 5% (m v^{-1}) skim milk in TBST for 1 h. Membranes were rinsed with rabbit anti-EGFP, rabbit anti-MTH1, rabbit anti-APE1, and rabbit anti-GAPDH primary antibody in TBST at 4 °C overnight. Membranes were then treated with the Horseradish Peroxidase (HRP)-labeled goat anti-rabbit secondary antibody for 2 h under room temperature. Finally, the western lightning enhanced chemiluminescence (ECL) substrate was loaded onto the membrane under dark conditions, and the fluorescence was monitored by enhanced chemiluminescence exposure. Protein expression was analyzed by grayscale analysis in Fig. 3e and 4f.

2.17. Immunofluorescence determination of intracellular MTH1 and APE1

1×10^5 A549 cells were seeded in a 24-well plate and cultured overnight. Then they were treated overnight by PBS, Cas9-APE1, Cas9-MTH1, Ce6-Ni-Cas9-MTH1, Ce6-Mn-Cas9-MTH1, Ce6-Mn-Cas9-APE1 and Ce6-Ni-Cas9-APE1. Herein, the amount of Cas9 is 7 μg per well and the molar ratio of Ce6 to Cas9 was 10 to 1. After 12 h, samples were treated with laser irradiation for 10 min and the cells were continue to culture for 24 h. The cells were cleaned twice with PBS and then fixed with 400 μL glutaraldehyde. After 20 min, it was rinsed with 0.2% (v v^{-1}) Triton X-100. After 15 min, it was treated with 300 μL 5%(m v^{-1}) BSA for 2 h. Then the corresponding primary antibody was added for 4 °C overnights and placed on a 30-rpm shaker for rinsing with PBS for three times. The secondary antibody was added and incubated for 1 h and CLSM observation was performed after DAPI staining. Data were exhibited in Fig. 4h. Blue channel: DAPI for nuclei; Green channel: Alexa Fluor 488 for MTH1 and APE1.

2.18. Animal experiments

All animal experiments were approved by the Ethics Committee of Tianjin University and were in accordance with the Animal Management Regulations of the Ministry of Health of the People's Republic of China. 6-week female nude mice (Beijing Huafkang Biotechnology Co, Ltd. Beijing, China) were subcutaneously inoculated with A549 tumor cells. After about 10 days, the tumor volume reached nearly 50 mm^3. 36 mice were randomly divided into six groups and treated by PBS, Ce6@F127, Ce6-Mn-Cas9-MTH1, Ce6-Mn-Cas9-APE1, Ce6-Ni-Cas9-APE1, and Ce6-Mn-Cas9-APE1 + MTH1 (sgRNA: 80 nM). Herein, Cas9 amount was 1 mg kg^{-1} per mouse and the molar ratio of Ce6 to Cas9 was 10 to 1. Laser

irradiation (660 nm, 0.1 W cm^{-2}, 15 min) was performed after intratumoral injection for 0.5 h in every group. Body weight and tumor volume were recorded every day. Size of tumors were quantified using formula $V = a \times b^2/2$, where a and b are tumor length and width, respectively. TV: Tumor Volume. RTV: Relative Tumor Volume. TGI = [1-RTV(The experimental group)/RTV(PBS group)] × 100%. Tumors and major organs were excised for further identification on 13 days as indicated. For H&E staining, specimens were fixed in formalin and sections embedded in paraffin. After sections were dewaxed, hematoxylin was stained for 10 min and eosin for 30 s. Images were taken using microscope and the results were shown in Fig. 5. All animal experimental procedures were supported by the Animal Experimental Ethics Committee of Tianjin University (License number: TJUE-2022-007).

2.19. Pharmacokinetics and biodistribution of Ce6-Mn-Cas9

To determine half-life in blood, free FITC-Cas9, Ce6-Mn-FITC-Cas9 with a dose of 0.08 mg of FITC labeled Cas9 were injected intravenously in CD-1 mice. The blood was collected at indicated time points (0.5 h, 1 h, 2 h, 4 h, 8 h, 24 h). 100 μL of serum were collected after centrifugation at 1000 *g* for 10 min and the supernatant was taken for fluorescence quantification with excitation/emission wavelengths at 480/520 nm. For biodistribution study, nude mice were intratumorally given FITC-labeled Ce6-Mn-Cas9 with 0.08 mg of FITC-Cas9 (molar ratio of Ce6 to Cas9 was 10 to 1). After 24 h of injection, mice were sacrificed and organs were collected and then imaged by IVIS (Night OWL II LB 983, Berthold Technologies) with excitation/emission wavelengths at 480/520 nm.

2.20. Toxicity evaluation of Ce6-Mn-Cas9 in vivo

To evaluate the toxicity of micelles in vivo, 5-week nude mice with tumors were injected Ce6-Mn-Cas9 intratumorally. The injection dose was 1 mg kg^{-1} each mouse (Cas9) and the molar ratio of Ce6 to Cas9 was 10:1. After 24 h of injection, blood was collected for blood test and major organs and tumors were removed and fixed for H&E staining.

3. Results and discussions

3.1. Preparation and characterization of Ce6-Mn@F127 micelles

Ce6, a commonly used photosensitizer, was selected to act as both a photosensitizer for PDT and a metal chelator. Various metals including Ni, Gd, Co, Mg, Zn, Ca, Cu, Mn were chelated into the Ce6 macrocycle center after encapsulation of Ce6 in aqueous Pluronic micelles. Metal chelation was verified by shifted absorbance maxima (Fig. S2a, Fig. 1a, and b) and slightly altered color (Fig. 1c) of different metal-chelated Ce6 micelles, with good chelation stability in serum (Fig. S2b). Pluronic micelles were used to increase the water solubility of metal-chelated Ce6, then His-tagged Cas9 was coupled to Ce6-metal@F127 micelles via coordination of metal and His-tag after incubation of Cas9 with micelles in aqueous solution. Pluronic F127 was found to have the higher yield than Pluronic F108 and F68, likely because it has longer poly(propylene oxide) (PPO) and poly(ethylene oxide) (PEO) blocks (Fig. S2c). Strikingly, Mn was found to enhance the endonuclease activity of Cas9 among the screened metals (Ni, Mn, Zn and Ca) as determined by agarose gel electrophoresis showing that the target gene (molecular weight of 738 bp) was cleaved only in the presence of Mn (Fig. 1d). The enhanced endonuclease activity by Mn^{2+} was concentration-dependent as shown in Fig. S2d. It has been reported that Mn^{2+}-dependent cleavage of CjeCas9 is catalyzed by the HNH domain, which has been shown to stabilize the surrounding protein residues and activated the HNH domain [43]. The catalytic activity of Cas9 can be improved by adjusting the concentration of Mn^{2+}, which is of significance for improving the effect of Cas9 gene editing and promoting its therapeutic application.

In order to verify the coupling of Cas9 to micelles, Cy3 and Cy5 were labeled on Cas9 and amine-modified F127, respectively, before generating Ce6-Mn@F127 micelles coordinated with Cas9 (termed Ce6-Mn-Cas9). As shown in Fig. 1e, after admixing Cas9 and Ce6-Mn@F127 micelles, the emission of the mixture at 570 nm (Cy3 emission maxima) became significantly quenched but the emission at 670 nm (Cy5 emission maxima) was enhanced when exciting Cy3, owing to

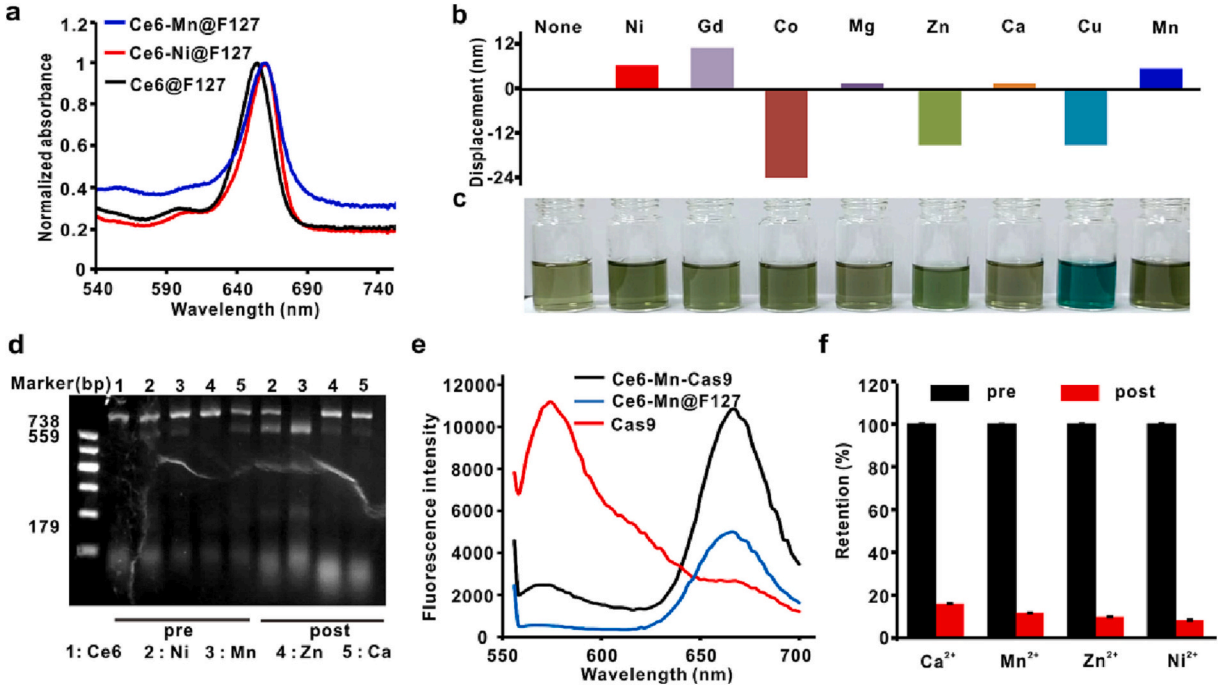

Fig. 1. Mn chelation with Ce6@F127 micelles for RNP delivery. (a) Absorbance spectra, (b) Absorbance maxima displacements, (c) Digital images of different metallo-Ce6@F127 micelles. (d) In vitro cleavage of target DNA by Cas9 in the presence of indicated metals. (e) FRET assay of Ce6-Mn-Cas9. Cas9 was labeled by Cy3, and Ce6@F127-NH_2 were labeled by Cy5. (f) Retention of fluorescence labeled Cas9 after treatment by imidazole and Triton X-100.

fluorescence resonance emission transfer (FRET) between Cy3 and Cy5, indicating the successful coupling of Cas9 to micelles. The FRET phenomenon was also observed for the case of Ce6-Ni-Cas9 (Fig. S3a). To further verify that Cas9 was attached to micelles by metal coordination, imidazole was added to Ce6-Mn-Cas9 to compete with the fluorescein isothiocyanate (FITC)-labeled Cas9, following centrifugation to remove free FITC-labeled Cas9. As shown in Fig. 1f, after imidazole treatment, the fluorescence of Ce6-metal-Cas9 significantly decreased due to competition with imidazole.

3.2. Preparation and characterization of Ce6-Mn-Cas9@F127 micelles

Next, we characterized the binding of Ce6-Mn-Cas9 by measuring the fluorescence quenching of FITC-labeled Cas9. We found no significant difference between different metallo micelles (Fig. 2a). Size was then characterized by dynamic light scattering (DLS). After coupling of Cas9, the size of Ce6-Mn@F127 micelles increased from 164 nm to 295 nm (Fig. 2b, S3b and S3c). Transmission electron microscopic images also showed similar size (Fig. S3d). The energy spectrum analysis verifies the presence of Mn (Fig. 2c), and the concentration of Mn ions in micelles was determined to be 40.28 mg mL^{-1} by ICP-OES.

Next, the photodynamic effect of Ce6-Mn-Cas9 was investigated using 1,3-diphenylisobenzofuran (DPBF) as a probe to assess the $^1O_2$ generation of Ce6-Mn@F127. Upon laser irradiation, the absorbance of the characteristic peak at DPBF at 420 nm decreased significantly, indicating that Ce6-Mn@F127 produced $^1O_2$ upon laser irradiation (Fig. 2d and S4c). Ce6-Ni@F127 had similar PDT effect (Fig. S4a, S4b and S4d). Electron spin resonance (ESR) of the 2,2,6,6-tetramethylpiperidine (TEMP)/$^1O_2$ adduct could be observed in the Ce6-Mn@F127 + laser group, but not in the Ce6-Mn@F127 or PBS groups (Fig. 2e and S4e). Besides Ce6, Mn ions can also produce ROS by Fenton-like effect, which was investigated using methylene blue (MB) as a probe since MB can be degraded by the Fenton-like effect. As shown in Fig. 2f and S4f, Ce6-Mn@F127 micelles induced significant Fenton-like effect compared to the controls of PBS and Ce6-Ni@F127.

Next, Cas9 release from the metal coordination micelles in a putative, simulated tumor biochemical environment was studied. As shown in Fig. 2g, 10 mM ATP, but not 0.1 mM ATP induced the complete release of FITC-labeled Cas9 within 6 h, since ATP has imidazole-like structure that compete withe for metal coordination. In addition, the metal in the center of the Ce6 macrocycle could be de-chelated at low pH. Therefore, as shown in Fig. 2h, Cas9 could be triggered released at pH 5.5 but not pH 7.4. As shown in the Fig. S5a, Ce6-Mn-Cas9 could be rapidly released in the simulated tumor intracellular environment with 10 mM ATP and pH of 5.5. In addition, in the presence of either 10 mM ATP, pH 5.5 or both, the size of micelles decreased from 190 nm to 91 nm, indicative of the release of Cas9 from micelles (Fig. S5b). This could be ascribed to the disruption of coordination of histidine and manganese due to the protonation of the histidine in the acidic conditions [44,45] and de-chelation of manganese from the center of Ce6 in the acidic

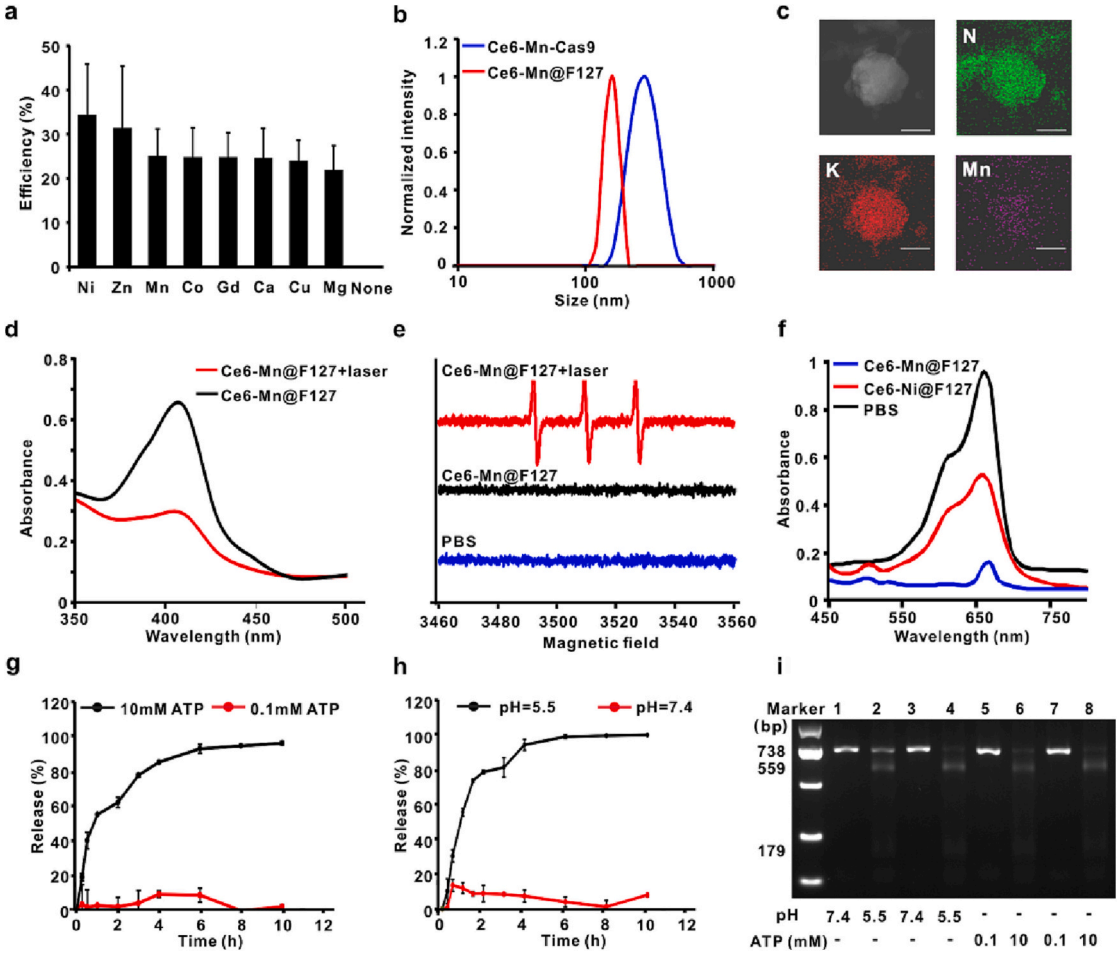

Fig. 2. Characterization of Ce6-Mn-Cas9 micelles. (a) The yield of Cas9 loaded by different metallo-Ce6@F127 micelles. (b) Size distributions. (c) TEM images and corresponding element mappings of Ce6-Mn-Cas9 (scale bar: 200 nm). (d) UV–Vis absorption spectra of DPBF after indicated treatment and (e) ESR spectra of Ce6-Mn-Cas9 in the absence and presence of laser irradiation (660 nm, 0.1 W cm^{-2}, 5 min). (f) Fenton-like degradation of MB in the presence of Ce6-Mn@F127 micelles and Ce6-Ni@F127 micelles. The (g) ATP and (h) pH-responsive release profiles of Ce6-Mn-Cas9 at different indicated conditions. (i) Gene editing of the released Cas9 determined by agarose gel electrophoresis.

condition [46,47]. We also found that 40% manganese was released at 12 h after treatment by acidic solutions of pH = 5.5 by ICP, as shown in Fig. S5c. In order to demonstrate that Cas9 retains its gene editing function after triggered release, the release profile and endonuclease activity of Ce6-Mn-Cas9 was studied by agarose gel electrophoresis (Fig. 2i) and sodium lauryl sulfate polyacrylamide gel electrophoresis (SDS-PAGE) (Fig. S5d). It was found that Cas9 attached on micelles were larger in size and could not pass through pores in electrophoresis gel. More importantly, the endonuclease activity could be restored only after Cas9 was released from micelles, which could be triggered in the conditions of pH of 5.5 or 10 mM ATP.

3.3. The intracellular PDT and gene-editing effect of Ce6-Mn-Cas9@F127

Next, we investigated the gene editing performance of Ce6-Mn-Cas9 at a cellular level. First, free Cas9, Ce6-Mn-Cas9 or Ce6-Ni-Cas9 were incubated with mouse embryonic fibroblast (NIH-3 T3) and human

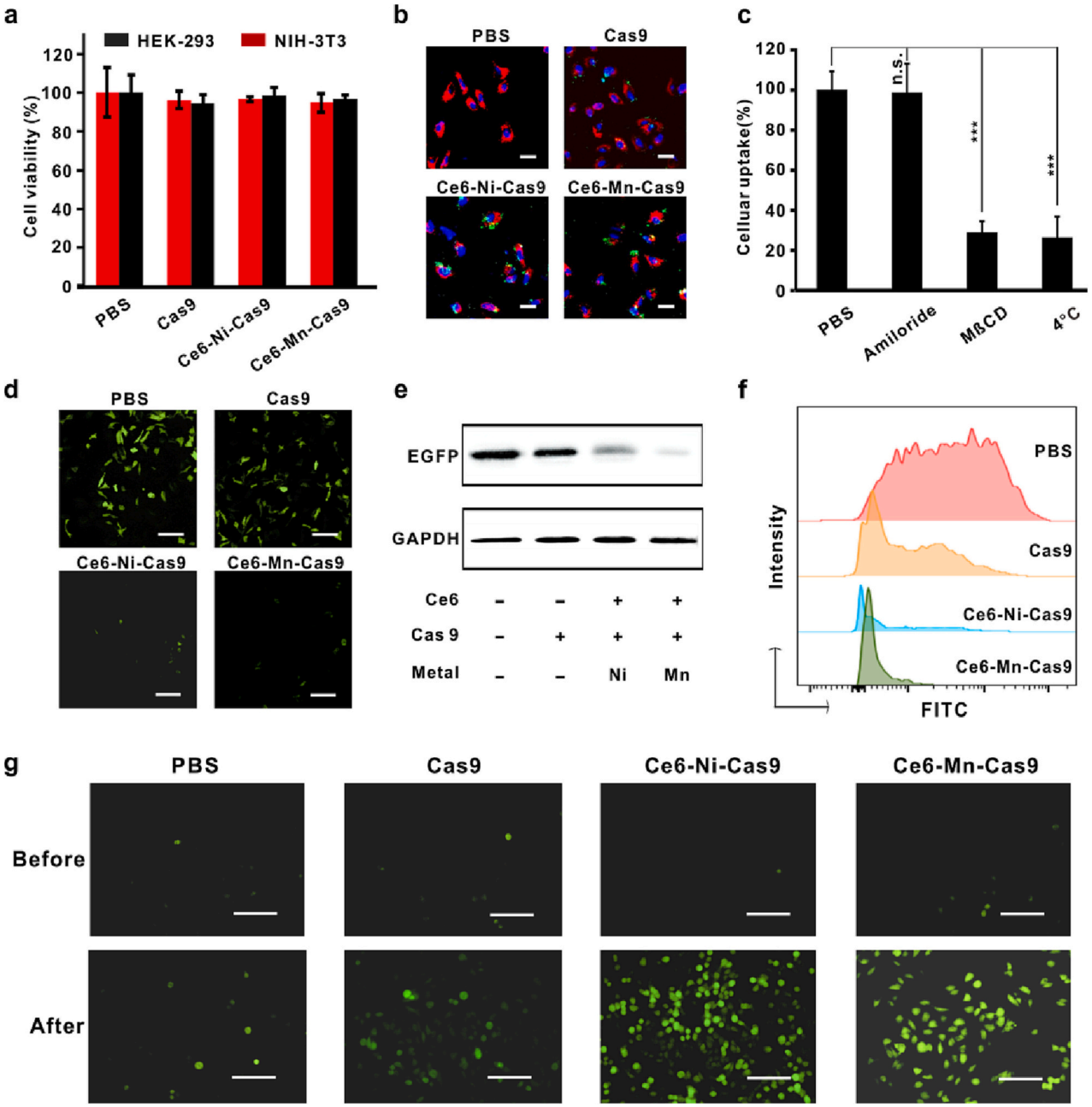

Fig. 3. Intracellular uptake of Ce6-Mn-Cas9 for PDT and EGFP gene editing in vitro. (a) Cytotoxicity of Ce6-Mn-Cas9, and controls including Ce6-Ni-Cas9, free Cas9 and PBS. HEK-293 cells and NIH-3 T3 cells were incubated with the sample overnight, followed by CCK-8 kit assay. ($n = 3$) (b) CLSM images of the intracellular distribution of the Cas9 complex. The nuclei and lysosomes were stained with Hoechst 33342 and LysoTracker Red, respectively, and the Cas9 complex was labeled with FITC (scale bar: 50 μm). (c) Cellular uptake of FITC-labeled Ce6-Mn-Cas9 treated with Methyl-β-cyclodextrin (MβCD), 5-(*N*, *N*-Hexamethylene)amiloride and low temperature. (n = 3) ** $p < 0.01$, *** $p < 0.001$, and **** $p < 0.0001$, analyzed by one-way ANOVA with Bonferroni's post hoc test. (d) CLSM images (scale bar: 100 μm) and (e) Western blot analysis of the EGFP expression in A549-EGFP cells treated with different samples (PBS, free Cas9-EGFP, Ce6-Ni-Cas9-EGFP and Ce6-Mn-Cas9-EGFP) (n = 3). (f) Flow cytometry analysis of A549-EGFP cells treated with different samples (PBS, Cas9-EGFP, Ce6-Ni-Cas9-EGFP and Ce6-Mn-Cas9-EGFP). Scale bar: 100 μm. (g) ROS generation after treatment by formulations as indicated upon laser irradiation (660 nm) under CLSM using DCFH-DA as indicator (scale bar: 100 μm). (For interpretation of the references to color in this figure legend, the reader is referred to the web version of this article.)

embryonic kidney (HEK-293) cells to assess its cytotoxicity. Fig. 3a shows that all these formulations had no significant cytotoxicity to cells as measured by a Cell Counting Kit-8 (CCK-8 kit) assay. Human pulmonary carcinoma (A549) cells were incubated with FITC-labeled free Cas9, Ce6-Ni-Cas9 and Ce6-Mn-Cas9 micelles for different times and it was found that cellular uptake of Ce6-Mn-Cas9 reached saturation at around 6 h, measured by the intracellular fluorescence (Fig. S6). Next, the cellular distribution of free Cas9, Ce6-Mn-Cas9 and Ce6-Ni-Cas9 was examined by confocal laser scanning microscope (CLSM) after co-incubation with A549 cells (Fig. 3b). Additional images in other

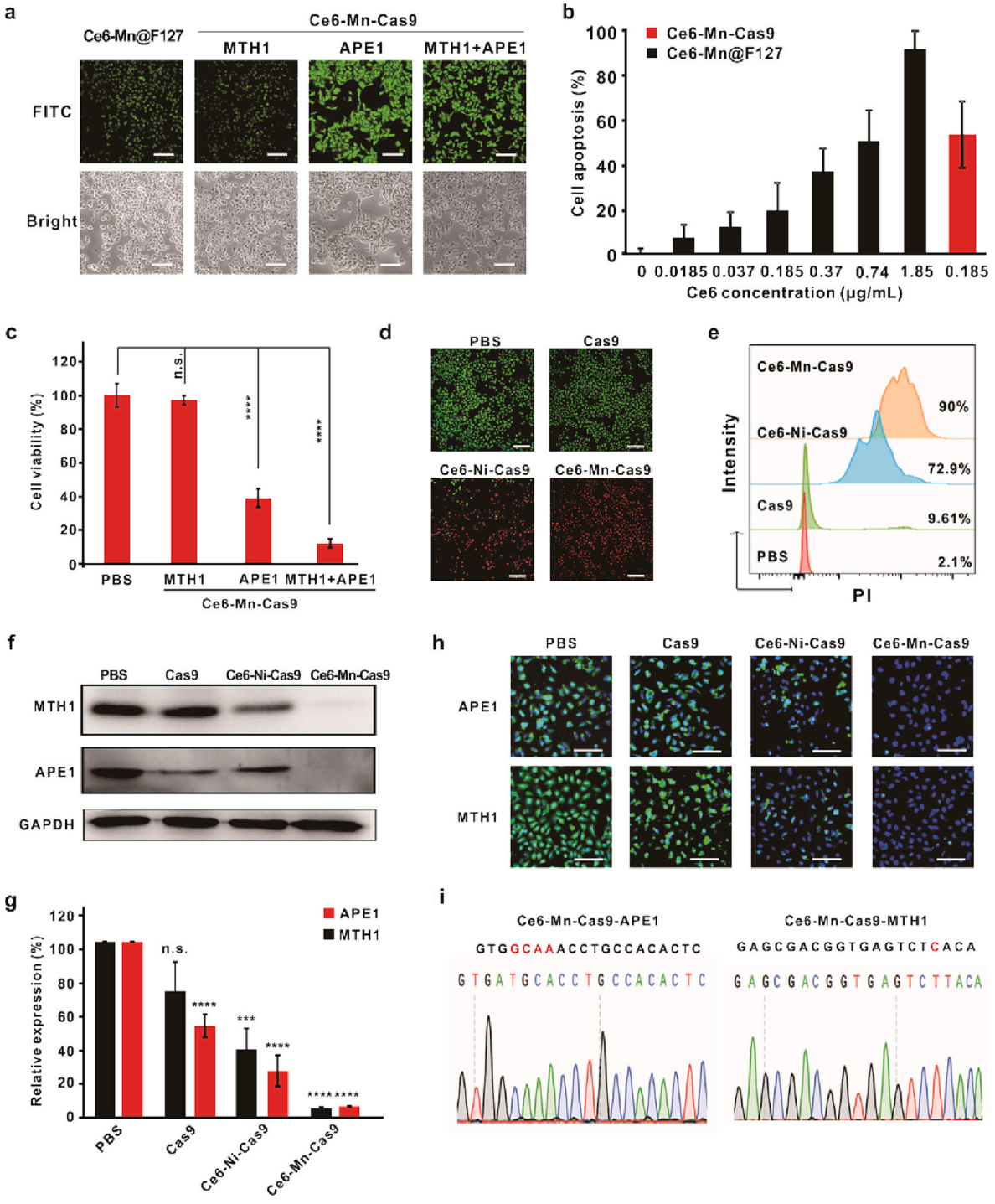

Fig. 4. SgRNA-mediated Cas9 delivery for enhanced ROS generation and gene editing. (a) CLSM observation of different micelles as indicated using DCFH-DA as ROS indicator (scale bar: 100 μm). (b) Cell viability of A549 cells treated by Ce6-Mn@F127 (0, 0.05, 0.1, 0. 5, 1, 2, 5 μg mL^{-1}) and Ce6-Mn-Cas9 (0.5 μg mL^{-1}) with laser irradiation (power density, 0.1 W cm^{-2}). (c) Cell viability of A549 cells treated by Ce6-Mn-Cas9 with different sgRNA combinations. (d) Live/dead staining analysis and (e) flow cytometry analysis of cells treated with different samples including Ce6-Mn-Cas9, as well as PBS, free Cas9 and Ce6-Ni-Cas9 as controls (with dual gRNAs for all). Scale bar: 200 μm. (f) Western blotting images and (g) corresponding quantitative analysis of APE1 and MTH1 proteins in A549 cells with different treatments ($n = 3$) including PBS, Cas9, Ce6-Ni-Cas9 and Ce6-Mn-Cas9. ** $p < 0.01$, *** $p < 0.001$, and **** $p < 0.0001$, analyzed by one-way ANOVA with Bonferroni's post hoc test. (h) Immunofluorescence images of APE1 and MTH1 in A549 cells after different treatments (scale bar: 100 μm). (i) Sanger sequencing analysis for the MTH1 and APE1 locus.

channels are shown in Fig. S7. The endocytosis pathways were also investigated by adding caveolae-dependent endocytosis inhibitor (MβCD), micropinocytosis-mediated endocytosis inhibitor (amiloride) or at low temperature (4 °C, as control). The uptake of FITC-labeled Cas9 was significantly reduced in the presence of Methyl-β-cyclodextrin (MβCD), suggesting that Ce6-Mn-Cas9 was ingested in cells by caveolae-dependent phagocytosis (Fig. 3c and S8) [48]. After confirming cellular uptake, the genome editing function of Ce6-Mn-Cas9 micelles was assessed. An A549 cell line expressing enhanced green fluorescent protein (EGFP) was used and incubated with Ce6-Mn-Cas9 with EGFP sgRNA (denoted as Ce6-Mn-Cas9-EGFP), as well as Ce6-Ni-Cas9-EGFP and free Cas9-EGFP as controls, followed by assessing green fluorescence expression with CLSM. As shown in Fig. 3d, only sporadic fluorescence could be seen from cells treated by Ce6-Mn-Cas9-EGFP or Ce6-Ni-Cas9-EGFP whereas A549 cells treated by PBS or free Cas9 expressed more fluorescence, suggesting that Ce6-Mn-Cas9 was an effective gene editing platform than other controls. The bright field channels are shown in Fig. S9. Furthermore, the concentration of EGFP collected from cells after treatment by Ce6-Mn-Cas9-EGFP and other controls was analyzed by western blot (WB) (Fig. 3e) and flow cytometry analysis (Fig. 3f). Ce6-Mn-Cas9-EGFP cleaved the EGFP gene, but the controls including free Cas9 and Ce6-Ni-Cas9-EGFP did not, leaving noticeable characteristic band and fluorescence signal of EGFP, confirming the effective genome editing in vitro of Ce6-Mn-Cas9-EGFP.

Next, intracellular ROS generated by Ce6-Mn-Cas9 upon laser irradiation was investigated in vitro using 2, 7-dichlorodihydrofluorescein diacetate (DCFH-DA) as a fluorescent ROS indicator. As shown in Fig. 3g, a green fluorescence signal from DCFH-DA was observed in A549 cells after incubation with Ce6-Mn-Cas9 and Ce6-Ni-Cas9 under laser irradiation compared with the PBS and free Cas9 groups where less green fluorescence signal could be seen. This suggests that $^1O_2$ could be effectively generated in vitro by Ce6-Mn-Cas9 under laser irradiation. In addition, $^1O_2$ did not affect the structural integrity and endonuclease activity of Cas9, as shown in Fig. S10.

3.4. Dual sgRNA Cas9 of ROS generation and gene editing reinforcement

After verifying the gene editing capability of the Ce6-Mn-Cas9 nanoplatform, we next used two therapeutic sgRNAs to mediate Ce6-Mn-Cas9 for gene and phototherapy. MTH1 sgRNA has been reported to be used to target antioxidant regulator but also leaves room for improvement for satisfactory results, therefore, we designed another gRNA used to suppress respiration and increase oxygen accumulation, which has not been used as sgRNA to mediate Cas9 before. The silencing of APE1 could partially inhibit mitochondrial function for accumulation of intracellular oxygen, eventually resulting in enhanced ROS production. MTH1 and APE1 sgRNAs were complexed separately or together with Ce6-Mn-Cas9 to generate Ce6-Mn-Cas9-MTH1, Ce6-Mn-Cas9-APE1 or Ce6-Mn-Cas9-MTH1 + APE1. As shown in Fig. 4a, after incubation with A549 cells, the newly designed APE1 gRNA could mediate Ce6-Mn-Cas9-APE1 to generate more ROS than MTH1, and the dual gRNAs provided the highest amount of ROS, which could directly give rise to significantly enhanced PDT efficacy.

Next, the photodynamictherapy efficacy of killing A549 cells using Ce6-Mn@F127 micelles or Ce6-Mn-Cas9 was investigated. The specific laser illumination time could be determined by Fig. S11, and the concentration of Ce6 was optimized to be 3 μg mL^{-1}. As shown in Fig. 4b, upon laser irradiation, 5 μg mL^{-1} Ce6-Mn@F127 micelles could kill over 90% A549 cells. In contrast, the presence of Cas9 complexed with dual gRNAs could effectively inhibit the cancer cell repair pathway and facilitate ROS excessive production, so that only 0.5 μg mL^{-1} Ce6-Mn-Cas9 could achieve similar therapeutic effect. In addition, as shown in Fig. 4c, the introduction of double sgRNA gave rise to improved therapeutic effect relative to single sgRNA. Thus, double sgRNAs were used in the following experiments unless noted otherwise. The live/dead staining of A549 cells was next conducted to assess the therapeutic effect of Ce6-Mn-Cas9, as well as PBS, free Cas9 and Ce6-Ni-Cas9 as controls (with dual gRNAs for all) after laser treatment. As depicted in Fig. 4d and e, Ce6-Mn-Cas9 and Ce6-Ni-Cas9 induced the death of 90% and 73% A549 cells, respectively (more images are shown in Fig. S12). In contrast, free Cas9 caused death of <10% cells with the most cells remaining green, indicative of live cells. The superior efficacy of Ce6-Mn-Cas9 over Ce6-Ni-Cas9 could be ascribed to the Fenton-like and cofactor effect of Mn, in consistence with the results in Fig. 2f.

In order to evaluate whether Ce6-Mn-Cas9-MTH1 + APE1 could effectively interfere with the expression of MTH1 and APE1 proteins in A549 cancer cells. A549 cells were treated with PBS, free Cas9, Ce6-Ni-Cas9 and Ce6-Mn-Cas9, respectively, followed by examination on the expression of MTH1 and APE1 in A549 cells by western blot (Fig. 4f and g). The expression of APE1, but not MTH1 was significantly decreased by free Cas9. Although Ce6-Ni-Cas9 + laser reduced the expression of both MTH1 and APE1 proteins, the expression of APE1 and MTH1 in cells treated with Ce6-Mn-Cas9 was significantly lower than other groups, which could be attributed to the Mn^{2+} acting as cofactor to promote Cas9 endonuclease activity. The amount of MTH1 and APE1 were also assessed by immunofluorescence staining. As shown in Fig. 4h, consistent with the results above, the expression of APE1 and MTH1 was significantly decreased after treatment by Ce6-Ni-Cas9 and Ce6-Mn-Cas9, but the latter induced the lowest protein expression than any other groups. More images are shown in Fig. S13. Additionally, Sanger sequencing was used to confirm the induced mutation at the MTH1 and APE1 locus (Fig. 4i).

3.5. The anti-tumor performance of Ce6-Mn-Cas9@F127

Encouraged by the effective anti-cancer therapy in vitro by Ce6-Mn-Cas9, we next set out to study its antitumor efficacy in vivo. Nude mice with 50 mm^3 tumor were randomly divided into six groups for different treatments including (I) PBS group, (II) Ce6@F127, (III) Ce6-Mn-Cas9-MTH1, (IV) Ce6-Ni-Cas9-APE1, (V) Ce6-Mn-Cas9-APE1 and (VI) Ce6-Mn-Cas9-MTH1 + APE1, the tumor volume and body weight of mice (6 mice for each group) were recorded every day during the treatment period (Fig. 5a). The tumor volume increase trend followed the order, from the least effective to most effective treatment of PBS, Ce6@F127, Ce6-Mn-Cas9-MTH1, Ce6-Ni-Cas9-APE1, Ce6-Mn-Cas9-APE1, Ce6-Mn-Cas9-MTH1 + APE1 (Fig. 5b, S14 and S15). The Ce6-Mn-Cas9-MTH1 + APE1 group had the slowest tumor growth rate compared with Ce6@F127 group, showing that the combination of gene and light therapy showed a stronger tumor therapeutic effect. The application of dual sgRNAs including MTH1 and APE1 also played an enhanced inhibition effect than single sgRNA alone. Ce6-Mn-Cas9-APE1 group showed slightly better tumor inhibition than that of Ce6-Ni-Cas9-APE1 because of the Fenton-like effect and cofactor effect of Mn, which agrees with the in vitro experiments. The cofactor effect of Mn^{2+}, but not Ni^{2+} for the endonuclease activity of Cas9 might be ascribed to the interaction of Mn^{2+} and RuvC or HNH structural domain [43]. For the Ce6-Mn-Cas9-MTH1 + APE1 group, a strong tumor suppressive effect was demonstrated especially within the first eight days, when the tumor volume was close to zero. The tumors were subsequently excised and tumor weights were recorded (Fig. 5c). Tumor growth inhibition of Ce6-Mn-Cas9-MTH1 + APE1 was up to 88% (Fig. 5d). No significant changes of the body weight of mice in all the groups was observed, suggesting that these formulations did not cause overt toxicity to mice (Fig. 5e). In addition, the efficacy of Ce6-Mn-Cas9-MTH1 + APE1 under laser irradiation was verified by hematoxylin-eosin staining (H&E staining). The cell density of tumor tissue in Ce6-Mn-Cas9-MTH1 + APE1 group was significantly lower than that in other groups with abnormal and incomplete cellular morphology (Fig. 5f). The pharmacokinetics (intravenous injection) and bio-distribution (intratumoral injection) in the mice bearing tumor were also studied. As shown in Fig. S16, Ce6-Mn-Cas9 had a longer half-life than free Cas9 after intravenous injection. Ce6-Mn-Cas9 was mostly retained in tumors after intratumoral

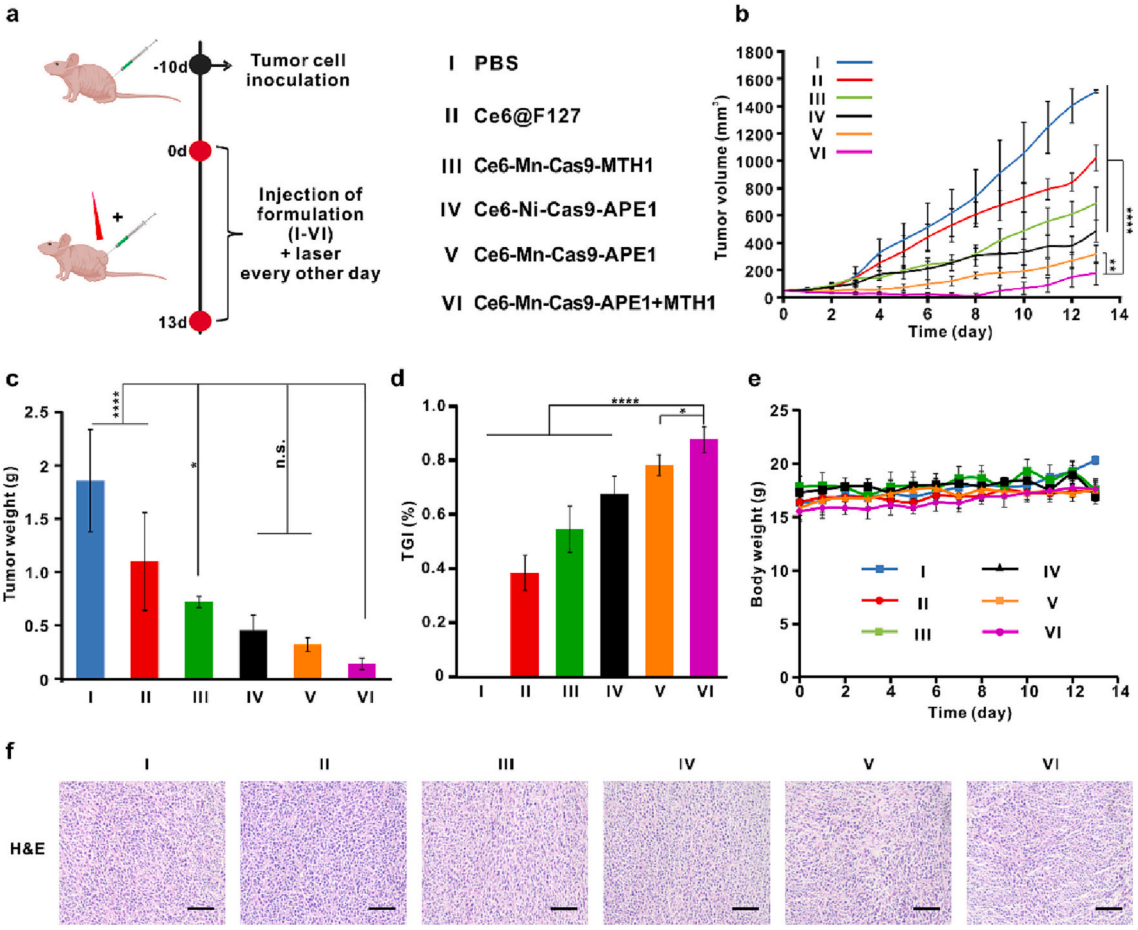

Fig. 5. In vivo antitumor efficacy of Ce6-Mn-Cas9. Mice were intratumorally injected by various formulations including PBS, Ce6@F127, Ce6-Mn-Cas9-MTH1, Ce6-Ni-Cas9-APE1, Ce6-Mn-Cas9-APE1 and Ce6-Mn-Cas9-MTH1 + APE1. 1 mg kg^{-1} (Cas9) was injected per mouse and the molar ratio of Ce6 to Cas9 was 10 to 1. (a) Treatment scheme of the Ce6-Mn-Cas9 therapeutic process. (b) Tumor volume (mm^3), (c) Weight of tumors, (d) TGI rate and (e) Body weights of mice at the end of the experiment after treatment by different formulations. (f) H&E staining of tumor tissues excised from mice treated by formulation I-VI. Scale bar: 100 μm. $n = 6$ for all groups. ** $p < 0.01$, *** $p < 0.001$, and **** $p < 0.0001$, analyzed by one-way ANOVA with Bonferroni's post hoc test.

injection (Fig. S17). To further evaluate the in vivo safety of Ce6-Mn-Cas9, hematology analysis and H&E staining of major organs mice treated by efficacy of dose of 1 mg kg^{-1} Cas9 were studied. As shown in Fig. S18, there was no significant difference for the complete blood count parameters between mice treated by PBS and Ce6-Mn-Cas9 including red blood cell count, platelet count, neutrophil (Neu) count, mean cell volume, and others. In H&E staining images, no obvious inflammation or lesions was observed in major organs including liver, heart, spleen, kidney and lung (Fig. S19), indicating that Ce6-Mn-Cas9 are highly biocompatible with no overt acute toxicity. It is also worth noting that the injection of Mn is about 0.83 mg kg^{-1}, which is much lower than the median lethal dose of $MnCl_2$ in mice (1715 mg kg^{-1}) and 10 mg manganese per day on typical Western diets as suggested for nutritional ingestions [49,50].

4. Conclusion

In summary, we developed a biochemically responsive nanoplatform for the delivery of the photosensitizer Ce6 and Cas9/sgRNA complexes for anti-cancer therapy. Mn chelation into Ce6 was critical for the activity of this approach. The co-delivery of Ce6 and Cas9 RNP targeting APE1 and MTH1 significantly enhanced antitumor effect through the following mechanisms: In the cytoplasmic microenvironment with acidic pH and abundant ATP, Cas9/sgRNA was triggered released. The cleavage of MTH1 proteins prevented MTH1 from protecting proliferating tumor cells and attenuating the damage caused by ROS, and APE1 protein impaired mitochondrial translation by damaging mRNA, resulting in reduced respiratory and enhanced oxygen accumulation. After NIR laser irradiation, PDT effect of Ce6 and Fenton-like effect of manganese both induced apoptosis of cancer cells. This nanoplatform not only exhibited enhanced efficacy of PDT with dual sgRNA, but also realized the controlled release and targeted therapy of CRISPR/Cas9 system. Altogether, Ce6-Mn-Cas9 holds potential for antitumor therapy through the combination of photo and gene therapy paradigms.

Author contributions

Conceptualization, Yumiao Zhang and Chen Zhang; Data curation, Chen Zhang and Xiaojie Wang; Formal analysis, Chen Zhang and Xiaojie Wang; Funding acquisition, Yumiao Zhang; Investigation, Yumiao Zhang and Chen Zhang; Methodology, Chen Zhang, Xiaojie Wang, Gengqi Liu, Zhen Jiang, He Ren, Jingang Liu and Jiexin Li; Project administration, Yumiao Zhang and Chen Zhang; Resources, Yumiao Zhang; Software Supervision, Xiaojie Wang and Gengqi Liu; Validation, Yumiao Zhang; Visualization, Chen Zhang and Xiaojie Wang; Writing - original draft, Chen Zhang, Xiaojie Wang; Writing - review & editing, Yumiao Zhang, Jiexin Li, Chen Zhang, Xiaojie Wang and Jonathan F Lovell.

Declaration of Competing Interest

The authors declare that they have no known competing financial

interests or personal relationships that could have appeared to influence the work reported in this paper.

Data availability

Data will be made available on request.

Acknowledgments

This work was supported by the National Natural Science Foundation of China (32071384), the National Key Research and Development Program (2021YFC2102300), Start-up Grant at Tianjin University and One-thousand Young Talent Program of China.

Appendix A. Supplementary data

Supplementary data to this article can be found online at https://doi.org/10.1016/j.jconrel.2023.03.042.

References

[1] Y. Liu, Y. Wang, S. Song, H. Zhang, Cancer therapeutic strategies based on metal ions, Chem. Sci. 12 (2021) 12234–12247.
[2] Y. Zhao, R. Li, J. Sun, Z. Zou, F. Wang, X. Liu, Multifunctional DNAzyme-anchored metal-organic framework for efficient suppression of tumor metastasis, ACS Nano 16 (4) (2022) 5404–5417.
[3] J. Li, H. Ren, Y. Zhang, Metal-based nano-vaccines for cancer immunotherapy, Coord. Chem. Rev. 455 (2022).
[4] J.X. Li, H. Ren, Y.P. Sun, G.Q. Liu, X.Y. Yang, Q. Qiu, Y.M. Ding, J.F. Lovell, Y. M. Zhang, Magnetic metal micelles for enhanced delivery of self-immolating CD8(+) T-cell epitopes for Cancer immunotherapy, Chem. Mater. 33 (2021) 9780–9794.
[5] X. Song, Q. Ding, J. Zhang, R. Sun, L. Yin, W. Wei, Y. Pu, S. Liu, Smart catalyzed hairpin assembly-induced DNAzyme Nanosystem for intracellular UDG imaging, Anal. Chem. 93 (2021) 13687–13693.
[6] H. Zhao, Z. Zhang, D. Zuo, L. Li, F. Li, D. Yang, A synergistic DNA-polydopamine-MnO_2 Nanocomplex for near-infrared-light-powered DNAzyme-mediated gene therapy, Nano Lett. 21 (2021) 5377–5385.
[7] Y. Huang, L.J. Ji, Q.C. Huang, D.G. Vassylyev, X.M. Chen, J.B. Ma, Structural insights into mechanisms of the small RNA methyltransferase HEN1, Nature 461 (2009) 823–U886.
[8] A.Y. Antipina, A.A. Gurtovenko, Toward understanding liposome-based siRNA delivery vectors: atomic-scale insight into siRNA lipid interactions, Langmuir 34 (2018) 8685–8693.
[9] M. Martinez-Pacheco, A. Hidalgo-Miranda, S. Romero-Cordoba, M. Valverde, E. Rojas, mRNA and miRNA expression patterns associated to pathways linked to metal mixture health effects, Gene 533 (2014) 508–514.
[10] Y.C. Zhao, J.Y. Xu, X.Y. Jiang, DNA cleavage and chemical transformation of nano-plastics mediated by surface ligand and size, Chem. Commun. 57 (2021) 9740–9743.
[11] Z. Zuo, J. Liu, Structure and dynamics of Cas9 HNH domain catalytic state, Sci. Rep. 7 (2017) 17271.
[12] R. Sundaresan, H.P. Parameshwaran, S.D. Yogesha, M.W. Keilbarth, R. Rajan, RNA-independent DNA cleavage activities of Cas9 and Cas12a, Cell Rep. 21 (2017) 3728–3739.
[13] C. Jia, Y. Guo, F.G. Wu, Chemodynamic therapy via Fenton and Fenton-like nanomaterials: strategies and recent advances, Small 18 (2022), e2103868.
[14] F. Li, Z.Y. Lv, X. Zhang, Y.H. Dong, X.H. Ding, Z.M. Li, S. Li, C. Yao, D.Y. Yang, Supramolecular self-assembled DNA Nanosystem for synergistic chemical and gene regulations on Cancer cells, Angew. Chem. Int. Edit. 60 (2021) 25557–25566.
[15] T. He, Y. Yuan, C. Jiang, N.T. Blum, J. He, P. Huang, J. Lin, Light-triggered transformable ferrous ion delivery system for Photothermal primed Chemodynamic therapy, Angew. Chem. Int. Ed. Eng. 60 (2021) 6047–6054.
[16] L.S. Lin, J. Song, L. Song, K. Ke, Y. Liu, Z. Zhou, Z. Shen, J. Li, Z. Yang, W. Tang, G. Niu, H.H. Yang, X. Chen, Simultaneous Fenton-like ion delivery and glutathione depletion by MnO_2-based Nanoagent to enhance Chemodynamic therapy, Angew. Chem. Int. Ed. Eng. 57 (2018) 4902–4906.
[17] S.Y. Yin, G. Song, Y. Yang, Y. Zhao, P. Wang, L.M. Zhu, X. Yin, X.B. Zhang, Persistent regulation of tumor microenvironment via circulating catalysis of $MnFe_2O_4$@metal–organic frameworks for enhanced photodynamic therapy, Adv. Funct. Mater. 29 (2019).
[18] V. Postupalenko, D. Desplancq, I. Orlov, Y. Arntz, D. Spehner, Y. Mely, B. P. Klaholz, P. Schultz, E. Weiss, G. Zuber, Protein delivery system containing a nickel-immobilized polymer for Multimerization of affinity-purified his-tagged proteins enhances cytosolic transfer, Angew. Chem. Int. Edit. 54 (2015) 10583–10586.
[19] R. Wieneke, R. Tampe, Multivalent chelators for in vivo protein labeling, Angew. Chem. Int. Ed. Eng. 58 (2019) 8278–8290.
[20] R. Xing, Q. Zou, C. Yuan, L. Zhao, R. Chang, X. Yan, Self-assembling endogenous Biliverdin as a versatile near-infrared Photothermal Nanoagent for Cancer Theranostics, Adv. Mater. 31 (2019), e1900822.
[21] J. Feng, Z. Xu, F. Liu, Y. Zhao, W. Yu, M. Pan, F. Wang, X. Liu, Versatile catalytic Deoxyribozyme vehicles for multimodal imaging-guided efficient gene regulation and Photothermal therapy, ACS Nano 12 (2018) 12888–12901.
[22] R.K. June, K. Gogoi, A. Eguchi, X.S. Cui, S.F. Dowdy, Synthesis of a pH-sensitive Nitrilotriacetic linker to peptide transduction domains to enable intracellular delivery of histidine imidazole ring-containing macromolecules, J. Am. Chem. Soc. 132 (2010) 10680–10682.
[23] Z.J. Yang, Y.J. Zhu, Z.L. Dong, Y. Hao, C.J. Wang, Q.G. Li, Y.M. Wu, L.Z. Feng, Z. Liu, Engineering bioluminescent bacteria to boost photodynamic therapy and systemic anti-tumor immunity for synergistic cancer treatment, Biomaterials 281 (2022).
[24] T. He, C. Jiang, J. He, Y. Zhang, G. He, J. Wu, J. Lin, X. Zhou, P. Huang, Manganese-dioxide-coating-instructed Plasmonic modulation of gold Nanorods for Activatable duplex-imaging-guided NIR-II Photothermal-Chemodynamic therapy, Adv. Mater. 33 (2021), e2008540.
[25] P. Liu, X. Shi, Y. Peng, J. Hu, J. Ding, W. Zhou, Anti-PD-L1 DNAzyme loaded Photothermal $Mn^{(2+)}$ /$Fe^{(3+)}$ hybrid metal-phenolic networks for cyclically amplified tumor Ferroptosis-immunotherapy, Adv. Healthc. Mater. 11 (2022), e2102315.
[26] Z. Dong, L. Feng, Y. Hao, Q. Li, M. Chen, Z. Yang, H. Zhao, Z. Liu, Synthesis of $CaCO_3$-based nanomedicine for enhanced Sonodynamic therapy via amplification of tumor oxidative stress, Chem 6 (2020) 1391–1407.
[27] Z.L. Zeng, C. Zhang, J.C. Li, D. Cui, Y.Y. Jiang, K.Y. Pu, Activatable polymer Nanoenzymes for photodynamic Immunometabolic Cancer therapy, Adv. Mater. 33 (2021).
[28] J. Lu, C. Ni, J. Huang, Y. Liu, Y. Tao, P. Hu, Y. Wang, S. Zheng, M. Shi, Biocompatible mesoporous silica-Polydopamine Nanocomplexes as MR/fluorescence imaging agent for light-activated Photothermal-photodynamic Cancer therapy in vivo, Front. Bioeng. Biotechnol. 9 (2021), 752982.
[29] Y.Y. Pu, H.H. Yin, C.H. Dong, H.J. Xiang, W.C. Wu, B.G. Zhou, D. Du, Y. Chen, H. X. Xu, Sono-controllable and ROS-sensitive CRISPR-Cas9 genome editing for augmented/synergistic ultrasound tumor Nanotherapy, Adv. Mater. 33 (2021).
[30] X.Y. Li, F.A. Deng, R.R. Zheng, L.S. Liu, Y.B. Liu, R.J. Kong, A.L. Chen, X.Y. Yu, S. Y. Li, H. Cheng, Carrier free photodynamic synergists for oxidative damage amplified tumor therapy, Small 17 (2021), e2102470.
[31] L. Huang, S. Zhao, J. Wu, L. Yu, N. Singh, K. Yang, M. Lan, P. Wang, J.S. Kim, Photodynamic therapy for hypoxic tumors: advances and perspectives, Coord. Chem. Rev. 438 (2021).
[32] D. Wang, H. Wu, S.Z.F. Phua, G. Yang, W. Qi Lim, L. Gu, C. Qian, H. Wang, Z. Guo, H. Chen, Y. Zhao, Self-assembled single-atom nanozyme for enhanced photodynamic therapy treatment of tumor, Nat. Commun. 11 (2020) 357.
[33] A. Barchiesi, V. Bazzani, A. Jabczynska, L.S. Borowski, S. Oeljeklaus, B. Warscheid, A. Chacinska, R.J. Szczesny, C. Vascotto, DNA repair protein APE1 degrades dysfunctional Abasic mRNA in mitochondria affecting oxidative phosphorylation, J. Mol. Biol. 433 (2021), 167125.
[34] F. Chen, M. Bai, K. Cao, Y. Zhao, J. Wei, Y. Zhao, Fabricating MnO_2 Nanozymes as intracellular catalytic DNA circuit generators for versatile imaging of base-excision repair in living cells, Adv. Funct. Mater. 27 (2017).
[35] N. Tang, Q. Ning, Z. Wang, Y. Tao, X. Zhao, S. Tang, Tumor microenvironment based stimuli-responsive CRISPR/Cas delivery systems: a viable platform for interventional approaches, Colloids Surf. B: Biointerfaces 210 (2022), 112257.
[36] L. Yu, Y. Chen, M. Wu, X. Cai, H. Yao, L. Zhang, H. Chen, J. Shi, Manganese extraction, strategy enables tumor-sensitive biodegradability and theranostics of nanoparticles, J. Am. Chem. Soc. 138 (2016) 9881–9894.
[37] D. Luo, K.A. Carter, D. Miranda, J.F. Lovell, Chemophototherapy: an emerging treatment option for solid tumors, Adv. Sci. (Weinh) 4 (2017) 1600106.
[38] T. Huang, T.Y. Zhang, X.C. Jiang, A. Li, Y.Q. Su, Q. Bian, H.H. Wu, R.Y. Lin, N. Li, H.C. Cao, D.S. Ling, J.Q. Wang, Y. Tabata, Z. Gu, J.Q. Gao, Iron oxide nanoparticles augment the intercellular mitochondrial transfer-mediated therapy, Sci. Adv. 7 (2021).
[39] R. Mout, M. Ray, Y.W. Lee, F. Scaletti, V.M. Rotello, In vivo delivery of CRISPR/Cas9 for therapeutic gene editing: Progress and challenges, Bioconjug. Chem. 28 (2017) 880–884.
[40] S. Tong, B. Moyo, C.M. Lee, K. Leong, G. Bao, Engineered materials for in vivo delivery of genome-editing machinery, Nat. Rev. Mater. 4 (2019) 726–737.
[41] C. Zhang, H. Ren, G.Q. Liu, J.X. Li, X.J. Wang, Y.M. Zhang, Effective genome editing using CRISPR-Cas9 Nanoflowers, Adv. Healthc. Mater. 11 (10) (2022).
[42] Y.M. Ding, B. Park, J.M. Ye, X.J. Wang, G.Q. Liu, X.Y. Yang, Z. Jiang, M. Han, Y. Fan, J.B. Song, C. Kim, Y.M. Zhang, Surfactant-stripped semiconducting polymer micelles for tumor Theranostics and deep tissue imaging in the NIR-II window, Small 18 (6) (2022).
[43] C. Saha, P. Mohanraju, A. Stubbs, G. Dugar, Y. Hoogstrate, G.J. Kremers, W.A. van Cappellen, D. Horst-Kreft, C. Laffeber, J.H.G. Lebbink, S. Bruens, D. Gaskin, D. Beerens, M. Klunder, R. Joosten, J.A.A. Demmers, D. van Gent, J.W. Mouton, P. J. van der Spek, J. van der Oost, P. van Baarlen, R. Louwen, Guide-free Cas9 from pathogenic campylobacter jejuni bacteria causes severe damage to DNA, Sci. Adv. 6 (2020).
[44] S. Shao, V. Rajendiran, J.F. Lovell, Metalloporphyrin nanoparticles: coordinating diverse theranostic functions, Coord. Chem. Rev. 379 (2019) 99–120.
[45] X.M. Yao, L. Chen, X.F. Chen, Z.G. Xie, J.X. Ding, C.L. He, J.P. Zhang, X.S. Chen, pH-responsive metallo-supramolecular nanogel for synergistic chemo-photodynamic therapy, Acta Biomater. 25 (2015) 162–171.
[46] Y.M. Zhang, D.P. Wang, S. Goel, B.Y. Sun, U. Chitgupi, J.M. Geng, H.Y. Sun, T. E. Barnhart, W.B. Cai, J. Xia, J.F. Lovell, Surfactant-stripped frozen Pheophytin micelles for multimodal gut imaging, Adv. Mater. 28 (2016) 8524–8530.

[47] X.F. Huang, K. Nakanishi, N. Berova, Porphyrins and metalloporphyrins: versatile circular dichroic reporter groups for structural studies, Chirality 12 (2000) 237–255.
[48] Z. Wang, W. Li, J. Park, K.M. Gonzalez, A.J. Scott, J. Lu, Camptothesome elicits immunogenic cell death to boost colorectal cancer immune checkpoint blockade, J. Control. Release 349 (2022) 929–939.
[49] J.L. Greger, Nutrition versus toxicology of manganese in humans: evaluation of potential biomarkers, Neurotoxicology 20 (1999) 205–212.
[50] R.J. Lewis, R.L. Tatken, Registry of Toxic Effects of Chemical Substances, US Department of Health and Human Services, National Institute for Occupational Safety and Health, 1980.